ACS OMEGA

http://pubs.acs.org/journal/acsodf

Article

Sulfonylated Indeno[1,2-*c*]quinoline Derivatives as Potent EGFR Tyrosine Kinase Inhibitors

Kowit Hengphasatporn,[○] Thitinan Aiebchun,[○] Panupong Mahalapbutr,* Atima Auepattanapong, Onnicha Khaikate, Kiattawee Choowongkomon,* Chutima Kuhakarn, Jatuporn Meesin, Yasuteru Shigeta,* and Thanyada Rungrotmongkol*

Cite This: *ACS Omega* 2023, 8, 19645−19655

Read Online

ACCESS | Metrics & More | Article Recommendations | Supporting Information

ABSTRACT: The epidermal growth factor receptor (EGFR) has been considered a potential target for lung cancer therapy due to its essential role in regulating the survival and proliferation of cancer cells. Although erlotinib, a potent EGFR tyrosine kinase (EGFR-TK) inhibitor, has been used as the first-line drug for lung cancer treatment, acquired drug resistance caused by the T790M secondary mutation of EGFR-TK inevitably develops after a median response duration of 9−13 months. Thus, the search for promising compounds to effectively target EGFR-TK has become an imperative necessity. In this study, the kinase inhibitory activities of a series of sulfonylated indeno[1,2-*c*]quinolines (SIQs) against EGFR-TK were experimentally and theoretically investigated. Among the 23 SIQ derivatives studied, eight compounds showed enhanced EGFR-TK inhibitory activity (IC_{50} values of ca. 0.6−10.2 nM) compared to the known drug erlotinib (IC_{50} of ∼20 nM). In a cell-based assay in human cancer cell lines with EGFR overexpression (A549 and A431 cells), the eight selected SIQs all showed more significant cytotoxicity against A431 than A549 cells, consistent with the higher EGFR expression in A431 cells. Molecular docking and FMO-RIMP2/PCM calculations revealed that SIQ17 occupies the ATP-binding site of EGFR-TK, where its sulfonyl group is mainly stabilized by C797, L718, and E762 residues. Triplicate 500 ns molecular dynamics (MD) simulations also confirmed the binding strength of SIQ17 in complex with EGFR. Overall, the potent SIQ compounds obtained in this work could be further optimized for developing novel anticancer drug candidates targeting EGFR-TK.

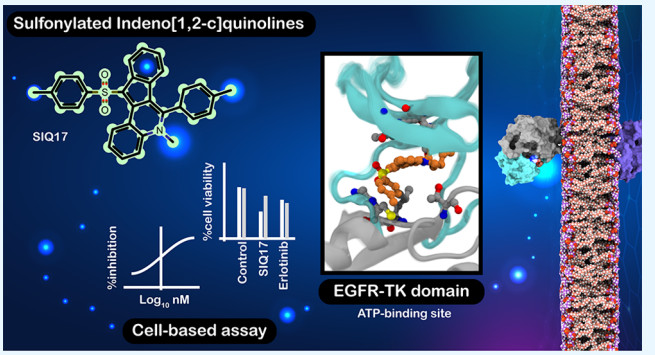

1. INTRODUCTION

Lung cancer is one of the most common diseases among humans, with a high mortality rate worldwide. Treatments for this form of cancer focus on inhibiting the formation and growth of tumors by targeting the relevant molecular targets.[1] Several targeted drugs have shown remarkable anticancer activity by explicitly blocking the driver oncogene-oriented signaling cascades. The epidermal growth factor receptor (EGFR) is a member of the ErbB family of tyrosine kinase receptors,[2] composed of an extracellular domain, a transmembrane region, and an intracellular tyrosine kinase (TK) domain.[3,4] The binding of epidermal growth factor (EGF) to the extracellular domain of EGFR results in conformational changes, which induces receptor dimerization with itself or with other proteins of the ErbB family and the subsequent phosphorylation of tyrosine. EGFR is considered one of the highly effective proteins for targeted cancer therapy due to relevant signaling cascades. This protein is overexpressed in many types of cancer, especially non-small-cell lung cancer (NSCLC),[5,6] and plays an essential role in regulating the proliferation, survival, differentiation, and apoptosis evasion of cancer cells.[7,8]

Erlotinib is one of the standard first-line treatments for EGFR mutation-driven NSCLC. Although this drug has been effective in cancer patients,[9,10] acquired drug resistance caused by the T790M secondary mutation in EGFR-TK inevitably develops after a median response duration of 9−13 months.[11] Additionally, erlotinib has several side effects, such as fatigue, paronychia, and hair changes.[12] Thus, the search for novel promising compounds that effectively target EGFR-TK has become an imperative necessity.[13,14] Erlotinib and other approved drugs targeting EGFR, including gefitinib and afatinib, as well as other reported compounds (IC_{50} of ca. 20−40 nM), are composed of a "quinoline ring".[15−17] As

Received: February 22, 2023
Accepted: May 5, 2023
Published: May 23, 2023

https://doi.org/10.1021/acsomega.3c01195
ACS Omega 2023, 8, 19645−19655

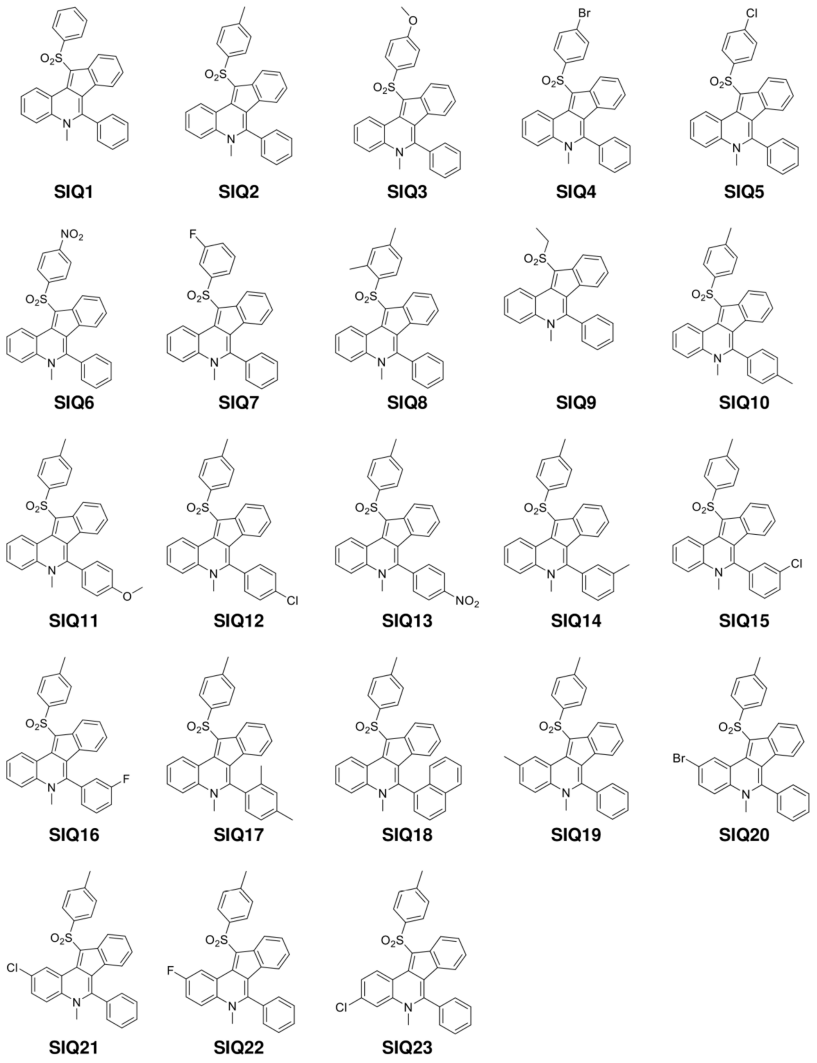

Figure 1. Chemical structures of 23 sulfonylated indeno[1,2-*c*]quinolines (SIQs) used in this study were obtained from ref 18.

sulfonylated indeno[1,2-*c*]quinolines (SIQs, Figure 1) contain the quinoline double-ring structure, we hypothesized that SIQs may inhibit EGFR-TK activity in a manner similar to the known EGFR inhibitors.

Traditional laboratory investigations require costly compound synthesis via a series of chemical methods and in vitro and in vivo experiments. In parallel with these, in silico studies provide a significant opportunity to design and develop novel potent inhibitors with desired specificity and sensitivity that can competitively inhibit the ATP-binding site of EGFR-TK. In this study, we propose a novel potent inhibitor based on the SIQ structures considered. The physicochemical properties and drug-likeness of a series of synthesized SIQs were first predicted, using computational tools to confirm their potential for successful development. Subsequently, these compounds were experimentally screened using the kinase inhibition assay against EGFR-TK. The in vitro cytotoxicity of the screened SIQs toward EGFR-overexpressing A549 and A431 cancer cells was determined using a 3-[4,5-dimethylthiazol-2-yl]-2,5 diphenyl tetrazolium bromide (MTT) assay and compared to that of erlotinib as a reference compound. The molecular binding mechanism of the potent SIQs was investigated via the fragment molecular orbital (FMO) method and molecular dynamics (MD) simulations. Per-residue free energy decomposition analysis revealed insights into the binding interaction profile and the manner in which the potent SIQs inhibit EGFR. Overall, the findings from this study could be advantageous in the further design and development of SIQ derivatives as novel anticancer drugs targeting EGFR-TK.

2. RESULTS AND DISCUSSION

2.1. Physicochemical Property Prediction. The drug-likeness of the 23 SIQs was predicted using ADMETlab 2.0 based on Lipinski's rule of five and their physicochemical properties.[19] The predicted ADMET profile showed that substituting Br in the SIQs increases their molecular weight (M_w), resulting in SIQ4 and SIQ20 falling outside of Lipinski's rule of five (M_w > 500 Da). In addition, the M_w of SIQ13 is slightly higher than 500 Da due to the methyl and NO_2 groups (Table 1). In contrast, the remaining SIQs are acceptable within the criteria of the physicochemical properties. Drug bioavailability can be computationally evaluated via predictions of lipophilicity (log *P*) and calculations of the topological polar surface area (TPSA). Apart from SIQ20 and SIQ21, most of the SIQs possess log *P* values in the range of −2 to 7 and TPSA values lower than 140 Å^2, indicating that the molecules can be passively absorbed via the gastrointestinal tract. The presence of the hydrophilic substituent NO_2 restricts

https://doi.org/10.1021/acsomega.3c01195
ACS Omega 2023, 8, 19645−19655

Table 1. Predicted Physicochemical Properties and Drug-Likeness of SIQ Derivatives

compounds	Lipinski[a]	M_w[b]	*n*HA[c]	*n*HD[d]	log *P*[e]	TPSA[f]	*n*Rot[g]	log S[h]
SIQ1	accepted	447.13	3	0	6.231	39.07	3	−7.921
SIQ2	accepted	447.13	3	0	6.231	39.07	3	−7.921
SIQ3	accepted	477.14	4	0	6.275	48.3	4	−8.073
SIQ4	rejected	525.04	3	0	6.778	39.07	3	−8.353
SIQ5	accepted	481.09	3	0	6.698	39.07	3	−8.256
SIQ6	accepted	492.11	6	0	6.150	82.21	4	−8.189
SIQ7	accepted	465.12	3	0	6.366	39.07	3	−8.038
SIQ8	accepted	475.16	3	0	6.757	39.07	3	−7.860
SIQ9	accepted	401.14	3	0	5.602	39.07	3	−7.529
SIQ10	accepted	475.16	3	0	6.858	39.07	3	−8.150
SIQ11	accepted	491.16	4	0	6.588	48.3	4	−8.174
SIQ12	accepted	495.11	3	0	6.993	39.07	3	−8.399
SIQ13	rejected	506.13	6	0	6.462	82.21	4	−8.348
SIQ14	accepted	463.16	3	0	6.652	39.07	3	−8.002
SIQ15	accepted	477.18	3	0	6.887	39.07	3	−8.075
SIQ16	accepted	497.12	3	0	6.891	39.07	3	−8.135
SIQ17	accepted	477.18	3	0	6.859	39.07	3	−8.128
SIQ18	accepted	463.16	3	0	6.652	39.07	3	−8.002
SIQ19	accepted	477.18	3	0	6.949	39.07	3	−8.100
SIQ20	rejected	541.07	3	0	7.123	39.07	3	−8.477
SIQ21	accepted	497.12	3	0	7.069	39.07	3	−8.376
SIQ22	accepted	481.15	3	0	6.728	39.07	3	−8.167
SIQ23	accepted	477.18	3	0	6.953	39.07	3	−8.078

[a]Lipinski = Lipinski's rule of five. [b]M_W = molecular weight (Da): ≤500. [c]*n*HA = number of hydrogen-bond acceptors: ≤10. [d]*n*HD = number of hydrogen-bond donors: ≤5. [e]log *P* = log of octanol-to-water partition coefficient: ≤5. [f]TPSA = topological polar surface area (Å^2): ≤140. [g]*n*Rot = number of rotatable bonds: ≤10. [h]log *S* = log of aqueous solubility (mol/L): −6 to 0.

permeation through the blood−brain barrier (BBB), as observed in SIQ6 and SIQ13. Although some compounds lie slightly outside of Lipinski's rule of five, all were selected for the experimental assay to confirm their EGFR inhibition activity.

2.2. Inhibition of EGFR-TK by SIQs. First, the EGFR-TK inhibitory activity of the 23 synthesized SIQs (Figure 1)[18] and erlotinib was measured at 1 μM to screen the potent SIQs. As shown in Figure 2, only eight compounds—SIQ3, SIQ5, SIQ8, SIQ10, SIQ11, SIQ12, SIQ17, and SIQ19—show higher EGFR-TK inhibitory activity than erlotinib. Thus, the half-maximal inhibitory concentration (IC_{50}) values of these eight SIQs were evaluated; six (SIQ3, SIQ5, SIQ8, SIQ12, SIQ17, and SIQ19; IC_{50} values of ca. 0.6−10.2 nM) exhibit higher EGFR-TK inhibitory activity than erlotinib, whereas SIQ10 (21.36 ± 5.74 nM) and SIQ11 (23.19 ± 8.76 nM) inhibit EGFR-TK in the same range as erlotinib (Figure 3). Notably, the EGFR-TK inhibitory activities of our compounds are higher than those of previously reported compounds containing quinoline (IC_{50} ranked from 0.003 to 10 μM),[20,21] indicating that SIQs could be promising compounds for the development of EGFR-TK inhibitors.

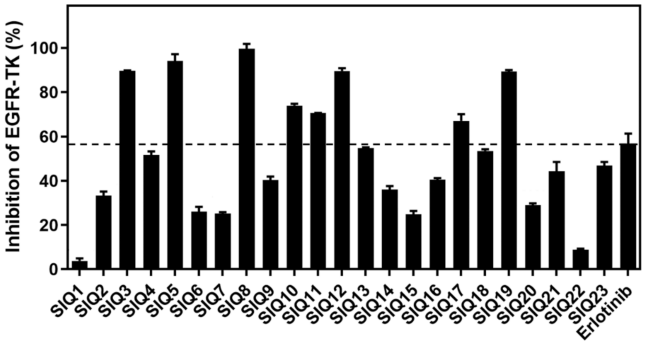

Figure 2. Kinase inhibitory activity screening of 23 SIQs toward EGFR-TK at 1 μM. The data are presented as the mean ± standard error of the mean (SEM) from duplicate independent experiments (n = 2).

2.3. Cytotoxicity. The eight selected SIQs from the kinase inhibition assay (Figure 3) were subjected to an in vitro cytotoxicity assay against the EGFR-overexpressing cancer cell lines A549 and A431. We found that the A549 cell line was more vulnerable to SIQ3, SIQ5, SIQ8, SIQ12, and SIQ17, whereas A431 was more susceptible to SIQ3, SIQ5, SIQ12, and SIQ19 (Figure 4). The six SIQs sensitive to both cell lines (SIQ3, SIQ5, SIQ8, SIQ12, SIQ17, and SIQ19) were selected for the calculation of IC_{50} values (Table 2). The results demonstrate that the cytotoxic effects of all of the selected compounds (IC_{50} of 16.8−33.5 and 9.9−19.2 μM) are somewhat similar to those of erlotinib (33.3 and 20.6 μM) against A549 and A431 cells. The cytotoxicity of the SIQs against A431 was higher than that against A549 due to (i) a higher EGFR expression level found in the A431 cells,[22] in good agreement with previous studies,[23,24] and (ii) the presence of KRAS mutations in the A549 cells, which constitutively activate downstream MAPK signaling pathways, leading to a compensatory mechanism.[25]

2.4. Fragment Molecular Orbital Calculations for Ligand−Protein Binding. Since SIQ17 shows the highest EGFR-TK inhibitory activity (Figure 3), we further investigated the binding mechanism between this compound and EGFR-TK using molecular docking followed by quantum mechanical (QM)-based pair interaction energy (PIE) calculations using the FMO-RIMP2/PCM method. The

https://doi.org/10.1021/acsomega.3c01195
ACS Omega 2023, 8, 19645−19655

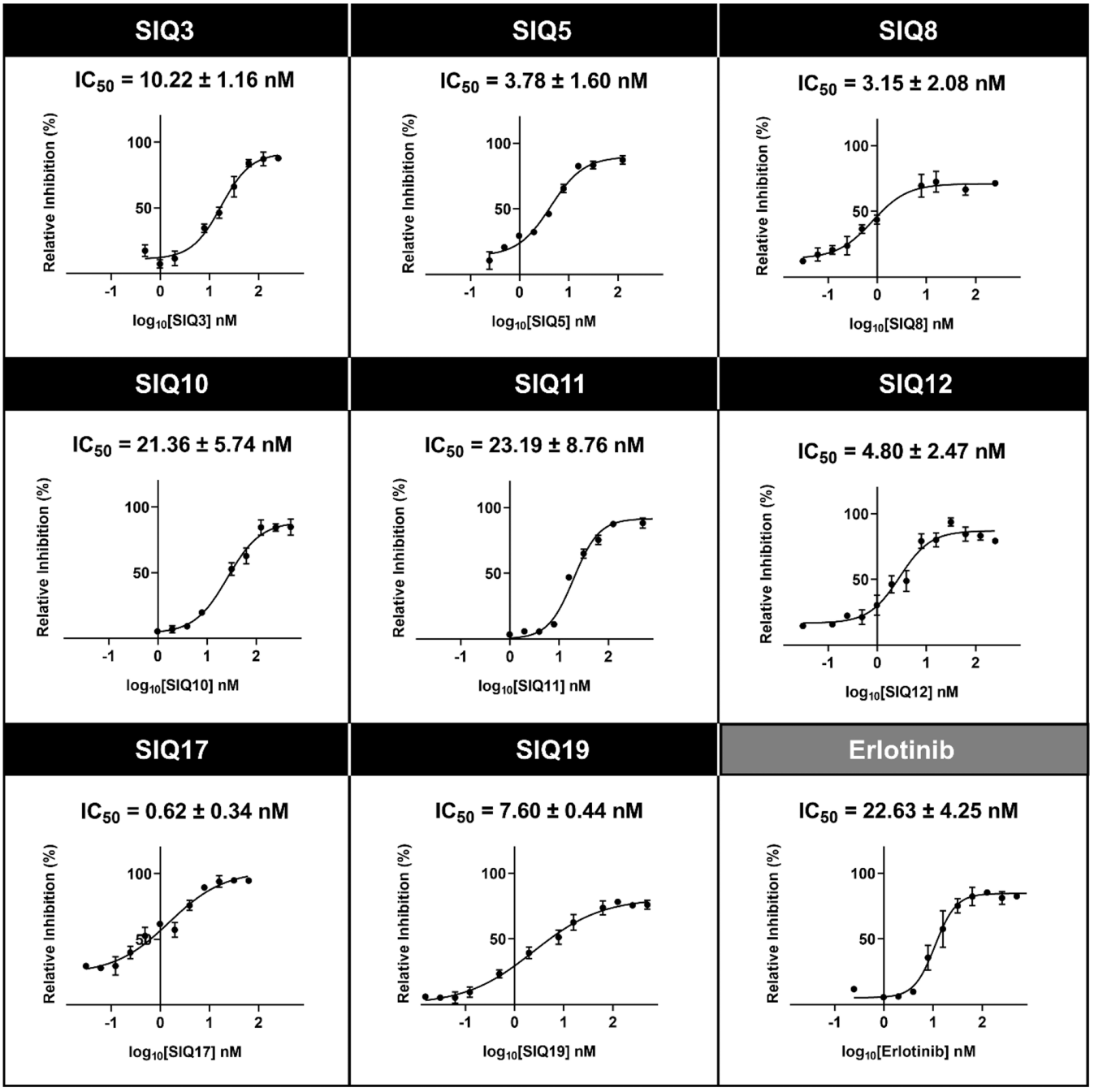

Figure 3. Kinase inhibitory activity of eight screened SIQs toward EGFR-TK. The data are presented as the mean ± SEM from triplicate independent experiments.

energy components of the PIE decomposition analysis (PIEDA) and the total PIE are illustrated in Figure 5 as a stacked bar graph and a grid spectrum, respectively. The PIE results reveal five components of the electronic properties of each interacting residue. The electrostatic (E_{ij}^{ES}) and charge transfer and mix (E_{ij}^{CT+mix}) terms are related to the salt-bridge, hydrogen-bond, and polar interactions. The dispersion (E_{ij}^{DI}) term represents hydrophobic interactions, while the exchange-repulsion (E_{ij}^{EX}) term involves the steric repulsion between electrons and the interacting atoms. The solvation free energy contribution is also considered using the polarizable continuum model (PCM; G_{Sol}^{PCM}). A computational study revealed the orientation of SIQ17, where the dimethyl indenoquinoline moiety is inserted deep within the ATP-binding pocket of EGFR while the toluene group is pointed outward (Figure 5). SIQ17 is trapped in this pocket via several interactions. The QM-FMO method was used to gain insights into the interaction, leading to the detection of three important residues residing in the ATP-binding pocket—L718 (P-loop), E762 (A-loop), and T854 (located close to the activation loop; A-loop)—that contribute to the binding of SIQ17 (PIE < −5.00 kcal/mol). SIQ17 mainly interacts with L718 and E762 via hydrophobic (E_{ij}^{DI}) and hydrogen bonding ($E_{ij}^{ES} + E_{ij}^{CT+mix}$) interactions, while G_{Sol}^{PCM} forms the major energy contribution between SIQ17 and T854. The core structure of SIQ17 is stabilized by E762 and T854, similar to the case for erlotinib.[26] Additionally, the dimethyl indenoquinoline moiety forms a cation−π interaction with K745, which has been reported as an

https://doi.org/10.1021/acsomega.3c01195
ACS Omega 2023, 8, 19645−19655

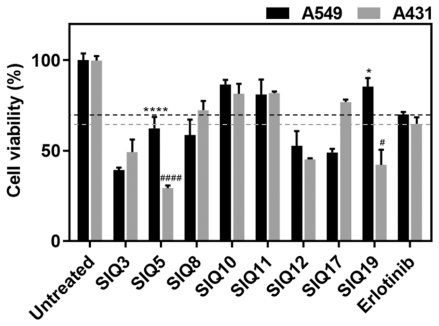

Figure 4. Cell viability of the A549 and A431 cell lines treated with SIQs and erlotinib at 10 μM for 72 h. The data are presented as the mean ± SEM (n = 3)—*$p \leq 0.05$ and ****$p \leq 0.0001$ versus erlotinib for A549, and $^{\#}p \leq 0.05$ and $^{\#\#\#\#}p \leq 0.0001$ versus erlotinib for A431.

Table 2. IC_{50} Values of SIQs against Cancer Cell Lines A549, A431, and Vero

	IC_{50} (μM)		
compounds	A549	A431	Vero
SIQ3	33.54 ± 0.47	17.67 ± 0.35	>100
SIQ5	16.84 ± 0.41	9.93 ± 0.45	8.06 ± 0.15
SIQ8	27.23 ± 0.71	14.10 ± 0.73	21.74 ± 0.50
SIQ12	23.25 ± 0.42	13.10 ± 0.50	7.25 ± 0.12
SIQ17	32.98 ± 0.59	19.17 ± 0.97	>100
SIQ19	29.31 ± 0.44	11.90 ± 0.41	5.88 ± 0.33
erlotinib	33.28 ± 1.88	20.57 ± 5.43	35.02 ± 1.35

important residue of EGFR.[27] The binding geometries of SIQ17 in the ATP-binding site reveal that its sulfonyl group is mainly stabilized by the conserved residue C797 via weak hydrogen bonding (see two-dimensional (2D) interaction in Figure 5), and an additional residue, L718, partially contributes to such binding via interactions with the sulfonyl group of SIQ17 (Figure 5). The contributions from L718, E762, and T854 residues have also been identified in previously reported EGFR-TK inhibitors such as chalcones,[28] anilino-1,4-naphthoquinones,[29] pyrimido[4,5-*b*]indoles,[30] and lycorine.[31]

2.5. Dynamics of SIQ17/EGFR Complex. To evaluate the binding mechanism and stability of SIQ17 in complex with EGFR-TK at the ATP-binding groove, we performed 500 ns MD simulations in triplicate (the trajectories are included in the Supporting Information). Although slight fluctuations of the toluene moiety in SIQ17 result in steep changes in the root-mean-square deviation (RMSD) plots early in the MD simulations, SIQ17 remains in its position in the ATP-binding region after rearrangement for up to 500 ns (Figure 6A), with RMSD fluctuations within ~0.5 Å. The radius of gyration (R_g) of the Cα atoms in the protein structure was analyzed to evaluate the system's compactness. The average R_g values gradually decrease and become stable after 400 ns. However, SIQ17 shows a high and stable number of atom contacts with the interacting residues in the ATP-binding pocket of EGFR-TK within a 7 Å sphere around SIQ17 during this period (Figure 7).

The conformational dynamics of the SIQ17/EGFR system were analyzed in triplicate using principal component analysis (PCA) and the MD trajectories from 400 to 500 ns. The scatter plots of the 3D positional Cartesian coordinates of PC1 and PC2 show how the stability of the system changes in this period (Figure 6B). Considering the covariance matrix of atomic fluctuations, the distributions of the structural dynamics among the three replications show a slightly different pattern due to the dynamics of the toluene moiety of SIQ17 in the third replication, where the protein motion shows better structural dynamics in the ATP-binding pocket. The fluctuations of the toluene moiety significantly affect the binding pose of SIQ17 in the ATP-binding site; however, neither the flipping-up nor flipping-down motion of toluene at the hinge region significantly affects the system stability.

2.6. Binding Affinity and Hot-Spot Residues. MM/PB(GB)SA is a computational method widely used to calculate the binding free energy of a complex system[32] using a combination of molecular mechanics and continuum solvent calculations. This method can be used to understand the energetics of SIQ17/EGFR interactions, with the binding free energy forming an important factor in drug design. The MD snapshots extracted from the last 100 ns of the trajectories of each system were used to perform the MM/PB(GB)SA calculations. As expected, hydrophobic interactions lead to a significant energetic contribution, as shown in the molecular mechanics (E_{MM}) terms, and, combined with the PB(GB) solvation energy, lead SIQ17 to reside in the ATP-binding pocket over the simulation time. However, the fluctuations of the toluene moiety in the third replication slightly affect the entropic terms (Table 3).

To further evaluate the key binding residues interacting with SIQ17, energy decomposition ($\Delta G^{bind}_{residue}$) analysis can be used to help elucidate the binding mode and mechanism of SIQ17 with regard to amino acids in the ATP-binding pocket. It can also confirm the stability of SIQ17 during the MD simulations by considering reasonable $\Delta G^{bind}_{residue}$ values from the important residues, such as L718, T854, and E762, in the initial structure of SIQ17/EGFR. Most of the considered key residues are identified in all replications, except for F723, G796, L792, C797, R841, and T854, which was caused by the different binding patterns of the toluene moiety in SIQ17. The flipped-up toluene configuration in the third replication results in an increased $\Delta G^{bind}_{residue}$ for F723 and a decreased value for L718. Moreover, the rearrangement of SIQ17 in this system enhances the interaction between the sulfonyl group and V726 via electrostatic and van der Waals forces. Overall, this finding could explain the structural factors supporting the in vitro EGFR inhibitory activity of the screened SIQ17.

3. CONCLUSIONS

This work combined experimental and computational techniques to identify novel potent EGFR inhibitors based on SIQ derivatives containing a quinoline core structure. First, the inhibitory activities of the 23 SIQ analogs against EGFR-TK were experimentally tested; eight compounds were found to inhibit EGFR-TK activity better than the approved drug erlotinib. From a cell-based assay in human cancer cell lines with EGFR overexpression (A549 and A431 cells), all eight compounds showed greater cytotoxicity against A431 than A549 cells, in accordance with a higher expression of EGFR in the former. Molecular docking and FMO-RIMP2/PCM calculations revealed that SIQ17 occupies the ATP-binding site, where its sulfonyl group is mainly stabilized by C797, L718, and E762 residues. Triplicate 500 ns MD simulations also confirmed the binding strength and dynamics of SIQ17 in complex with EGFR, where the core structure is maintained tightly in the ATP-binding site, in good agreement with the experimental study. SIQ17 could be further optimized and

https://doi.org/10.1021/acsomega.3c01195
ACS Omega 2023, 8, 19645−19655

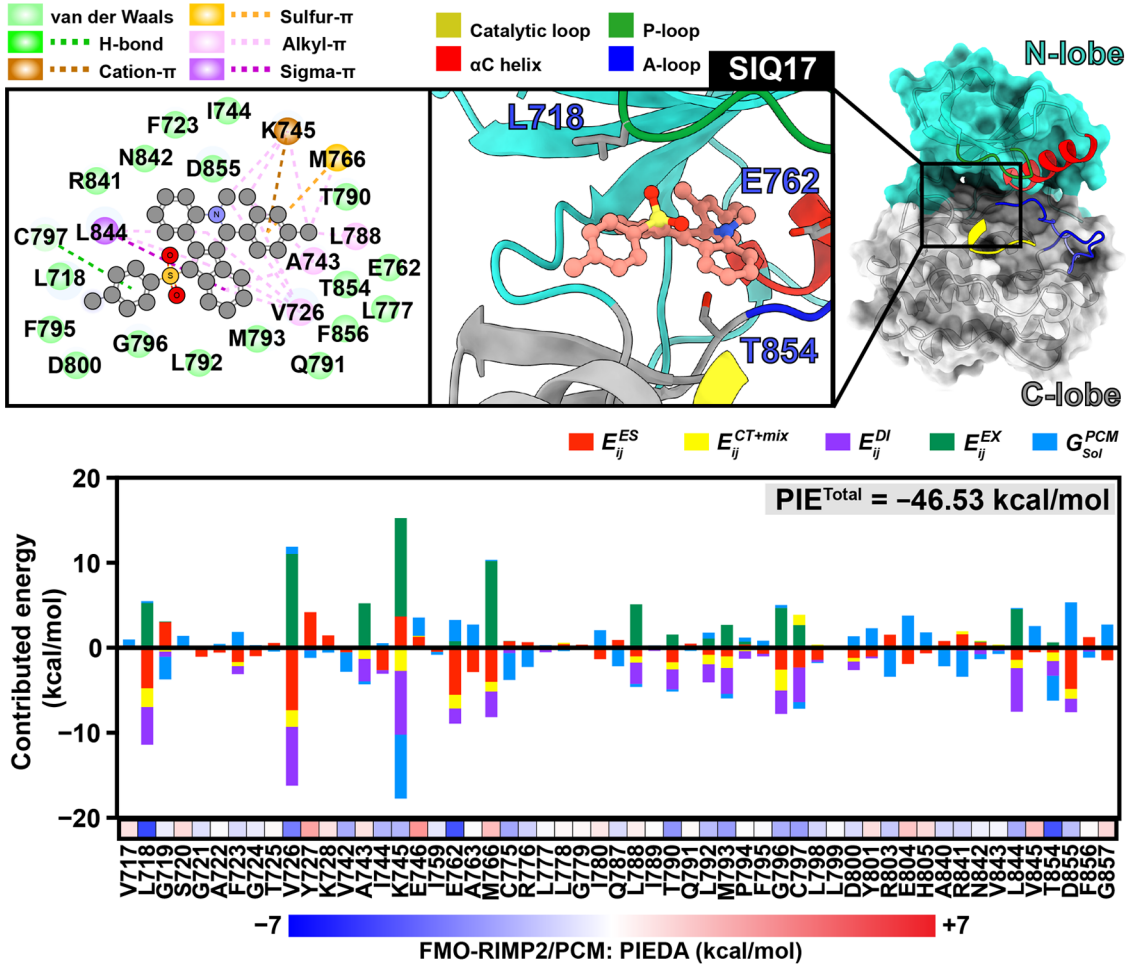

Figure 5. Ligand orientation and interactions in the ATP-binding pocket of EGFR-TK, where the residues with PIE < −5 kcal/mol are colored based on the spectrum bar and the total PIE. The energy components are illustrated in the grid diagram and stacked bar graph. The electrostatic (E_{ij}^{ES}), charge transfer and mix (E_{ij}^{CT+mix}), dispersion (E_{ij}^{DI}), exchange-repulsion (E_{ij}^{EX}), and PCM solvation (G_{Sol}^{PCM}) contributions are indicated in red, yellow, purple, green, and blue, respectively.

tested in an animal model for the development of novel anticancer drug candidates targeting EGFR-TK.

4. MATERIALS AND METHODS

4.1. Physicochemical Property Prediction. The 2D structure of 23 sulfonylated indeno[1,2-*c*]quinolines (SIQs) was constructed in the simplified molecular-input line-entry system (SMILES) format using Marvin version 21.17.0, Chemaxon (https://www.chemaxon.com). In this study, the physicochemical properties included Lipinski's rule of five, molecular weight (M_W), number of hydrogen-bond acceptors (*n*HA), number of hydrogen-bond donors (*n*HD), lipophilicity prediction (log P), topological polar surface area (TPSA), number of rotatable bonds (*n*Rot), and solubility (log S), which were calculated for the 23 SIQs using ADMETlab 2.0.[19]

4.2. Chemical Reagents and Cell Lines. The ADP-Glo Kinase Assay kit was purchased from Promega (Wisconsin). The investigated series of SIQ derivatives were provided by Chutima Kuhakarn from the Department of Chemistry and Center of Excellence for Innovation in Chemistry (PERCH-CIC), Faculty of Science, Mahidol University.[18] The lung carcinoma A549 (ATCC CCL-185) and epidermoid carcinoma A431 (ATCC CRL-1555) cell lines were purchased from the American Type Culture Collection (ATCC, Manassas, VA). Dulbecco's modified Eagle's medium (DMEM), fetal bovine serum (FBS), penicillin-streptomycin (Pen-Strep), and trypsin were purchased from Life Technologies (California). 3-(4,5-Dimethylthiazol-2-yl)-2,5-diphenyl tetrazolium bromide (MTT) and dimethyl sulfoxide (DMSO) were purchased from Sigma-Aldrich (Darmstadt, Germany).

4.3. Inhibition of EGFR-TK by Vinyl Sulfone Derivatives. A series of SIQs were screened for their ability to inhibit the tyrosine kinase activity of EGFR using the ADP-Glo Kinase Assay, as previously reported.[33,34] First, 8 μL of a buffer (40 mM Tris-HCl at pH 7.5, 20 mM $MgCl_2$, and 0.1 mg/mL bovine serum albumin) was added to a 384-well plate. Subsequently, 5 μL of EGFR enzyme (1.25 ng/μL) and 2 μL of inhibitors were added, followed by 10 μL of a mixture of 5 μM ATP and 2.5 μM poly(Glu-Tyr); the plate was then incubated for 1 h at room temperature. Next, 5 μL of the ADP-Glo reagent was added, followed by incubation for 40 min. Thereafter, 10 μL of the kinase detection reagent was added, and the plate was incubated at room temperature for 30 min to convert the ADP to ATP. The ATP was then detected by measuring the luminescence using a microplate reader (Infinite M200 microplate reader, Tecan, Männedorf, Switzerland). All assays were performed in triplicate. The relative inhibition (%)

https://doi.org/10.1021/acsomega.3c01195
ACS Omega 2023, 8, 19645−19655

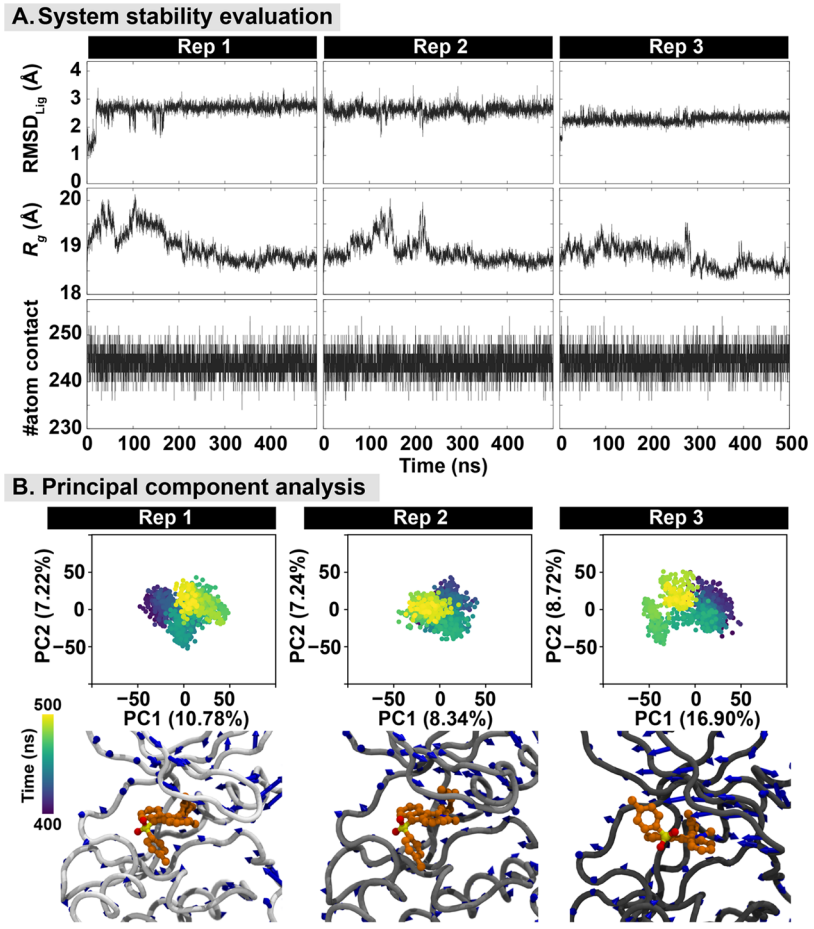

Figure 6. (A) RMSD, radius of gyration (R_g), and number of atom contacts (#atom contact) for SIQ17 in complex with the ATP-binding site of EGFR plotted as a function of the simulation time. (B) (Top) Two-dimensional projection of the PC1 and PC2 modes for the SIQ17/EGFR complexes analyzed in the last 100 ns of the MD trajectories. (Bottom) Comparison of the protein dynamics from the three replications (light gray, gray, and dim gray) along the PC1 and PC2 eigenvectors using porcupine plots, represented by the blue arrows.

of the inhibitors was then calculated in comparison to the control with no inhibitor, as shown in eq 1

$$\%\ \text{relative inhibition} = \frac{[(\text{positive} - \text{negative}) - (\text{sample} - \text{negative})]}{(\text{positive} - \text{negative})} \times 100 \quad (1)$$

4.4. Cell Cultures. The A549, A431, and Vero cells were grown completely in DMEM supplemented with 10% (v/v) FBS, 100 U/mL penicillin, and 100 μg/mL streptomycin. All cells were maintained at 37 °C in a 5% (v/v) CO_2, 95% (v/v) air-humidified incubator.

4.5. Cytotoxicity in Cancer Cell Lines and Normal Cell Lines. The in vitro cytotoxicity activity of SIQ derivatives against the A549, A431, and Vero cell lines was evaluated using the MTT assay. First, 100 μL of A549 (5000 cells/well), A431 (5000 cells/well), and Vero (4000 cells/well) cell suspensions were seeded per well in a 96-well microplate and incubated at 37 °C overnight; the cells were then treated with different concentrations of the SIQ compounds and the known drug (erlotinib) and incubated for 72 h. Subsequently, the MTT solution (5 mg/mL) was added to the A549, A431, and Vero cells, and the plate was incubated at 37 °C for 3 h. The medium was removed, and 50 μL of DMSO was added to each well to lyse the cells. Finally, the absorbance was measured at 570 nm using a microplate reader (Infinite M200 microplate reader, Tecan, Männedorf, Switzerland).

4.6. Statistical Analysis. The data are presented as the mean ± standard error of the mean (SEM). The differences between groups were compared using a one-way ANOVA, followed by Tukey's test for multiple comparisons. The differences in the means were determined at a significance level of $P \leq 0.05$.

4.7. Molecular Docking and Fragment Molecular Orbital Method. Molecular docking was used to construct the initial structures for the ab initio QM-based interaction energy calculations using the FMO method. The crystal structure of EGFR complexed with erlotinib (PDB ID: 1M17)[35] was retrieved from the Protein Data Bank (PDB). The 3D structure of SIQ17 was generated using GaussView 5.[36] SIQ17 was then optimized using the Gaussian 09 program with the HF/6-31d basis set, as previously reported.[37−39] The protonation state of SIQ17 was characterized using the pKa calculation implemented in Marvin version 21.17.0, Chemaxon (https://www.chemaxon.com). The binding site of erlotinib in the EGFR crystal structure was defined as a docking sphere (15 Å) for molecular docking using the CDOCKER program[40] with 100 independent runs. The binding mode between EGFR and SIQ17 was visualized using Accelrys Discovery Studio 3.0 (Accelrys, Inc.) and the UCSF Chimera package.[41] The complex of each system with the lowest CDOCKER

https://doi.org/10.1021/acsomega.3c01195
ACS Omega 2023, 8, 19645−19655

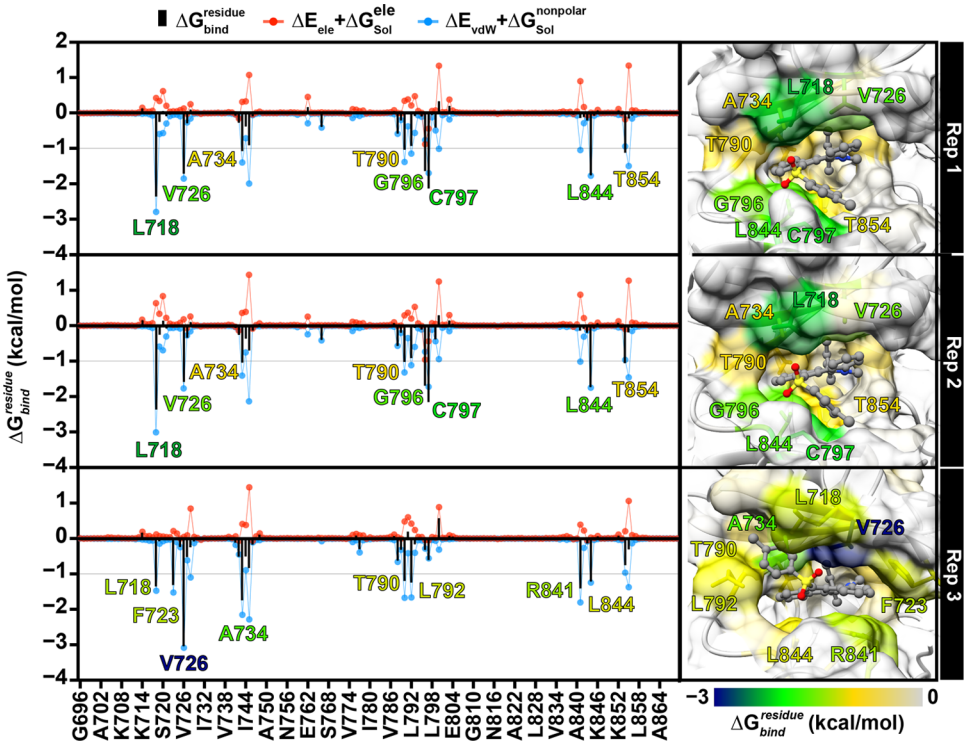

Figure 7. Interaction energy profile of the SIQ17/EGFR complexes (analyzed in triplicate) calculated via per-residue free energy decomposition analysis based on the MM/GBSA method using 100 snapshots extracted from the last 100 ns of the simulations. The interacting residues in the plots and three-dimensional (3D) structures with energy contributions ≤ −1 kcal/mol are labeled and colored according to their contributions.

Table 3. MM/PB(GB)SA-Calculated Binding Free Energy and Energy Components (kcal/mol) for the Triplicate Trajectories of SIQ17 Binding to EGFR at the ATP-Binding Site

	Rep 1	Rep 2	Rep 3
ΔE_{vdW}	−51.41 ± 0.33	−53.25 ± 0.27	−52.07 ± 0.28
ΔE_{ele}	−10.58 ± 0.45	−3.53 ± 0.23	−18.66 ± 0.40
ΔE_{MM}	−61.70 ± 0.63	−56.78 ± 0.37	−70.73 ± 0.52
$-T\Delta S$	20.53 ± 3.40	22.68 ± 3.19	24.66 ± 1.69
$\Delta G_{Sol}^{PB/ele}$	37.53 ± 0.60	27.98 ± 0.34	43.97 ± 0.50
$\Delta G_{Sol}^{PB/nonpolar}$	−7.60 ± 0.03	−7.72 ± 0.02	−7.24 ± 0.02
ΔG_{Sol}^{PB}	29.93 ± 0.58	20.26 ± 0.33	36.74 ± 0.49
$\Delta G_{Total}^{MM/PBSA}$	−32.07 ± 0.33	−36.52 ± 0.28	−34.00 ± 0.36
$\Delta G_{Bind}^{MM/PBSA}$	−11.54 ± 1.54	−13.84 ± 1.30	−9.33 ± 0.90
$\Delta G_{Sol}^{GB/ele}$	30.97 ± 0.51	24.52 ± 0.25	38.05 ± 0.43
$\Delta G_{Sol}^{GB/nonpolar}$	−4.54 ± 0.03	−4.67 ± 0.02	−4.64 ± 0.02
ΔG_{Sol}^{GB}	26.44 ± 0.50	19.85 ± 0.24	33.41 ± 0.42
$\Delta G_{Total}^{MM/GBSA}$	−35.55 ± 0.30	−36.93 ± 0.28	−37.32 ± 0.29
$\Delta G_{Bind}^{MM/GBSA}$	−15.03 ± 1.51	−14.25 ± 1.27	−12.66 ± 0.88

interaction energy was selected as the initial structure for FMO calculations.

The PIE of the consensus residues of EGFR within a 7 Å radius of SIQ17 was determined by calculating the electronic energy components—electrostatic interaction (E_{ij}^{ES}), charge transfer with higher-order mixed term energies (E_{ij}^{CT+mix}), dispersion interaction (E_{ij}^{DI}), and exchange-repulsion energy (E_{ij}^{EX})—between each pair of the fragment (i and j). This was done by using the resolution-of-the-identity second-order Møller−Plesset perturbation theory (RIMP2) combined with the PCM (G_{Sol}^{PCM}) to describe the solvation effects, as given in eq 2, which was implemented in the GAMESS software[42−47]

$$\text{PIE} = \Delta E_{ij}^{ES} + \Delta E_{ij}^{CT+mix} + \Delta E_{ij}^{DI} + \Delta E_{ij}^{EX} + \Delta G_{Sol}^{PCM} \quad (2)$$

4.8. Molecular Dynamics Simulations. To evaluate the structural dynamics of the SIQ17/EGFR complex, the docked structure was used to perform the MD simulations using the AMBER20 package. The complex structure was prepared and placed in a periodic box using the TIP3P water model with a spacing distance of 15 Å from the EGFR surface, using the tleap module of AmberTools21. The system was neutralized by adding ions and then minimized and structurally relaxed using harmonic potentials, according to the standard protocols used in previous studies. The system was simulated for 500 ns in triplicate, and the system stability was represented by the changes in the RMSD, R_g, and number of atom contacts during the simulation. MD snapshots extracted from the last 100 ns of the trajectories of each system were analyzed with PCA and binding free energy calculations using the program CPPTRAJ and MMPBSA.py in AMBER20. MD trajectories were attached to Supporting Information.

■ ASSOCIATED CONTENT

Supporting Information

The Supporting Information is available free of charge at https://pubs.acs.org/doi/10.1021/acsomega.3c01195.

Simplified molecular-input line-entry system (SMILES) format for 23 SIQs; procedure and characterization data (PDF)

Compounds (XLS)

500 ns MD trajectories for the first of three replications (MOV)

500 ns MD trajectories for the second of three replications (MOV)

https://doi.org/10.1021/acsomega.3c01195
ACS Omega 2023, 8, 19645−19655

500 ns MD trajectories for the third of three replications (MOV)

AUTHOR INFORMATION

Corresponding Authors

Panupong Mahalapbutr − *Department of Biochemistry, Faculty of Medicine, Khon Kaen University, Khon Kaen 40002, Thailand;* orcid.org/0000-0003-4389-334X; Email: panupma@kku.ac.th

Kiattawee Choowongkomon − *Department of Biochemistry, Faculty of Science, Kasetsart University, Bangkok 10900, Thailand;* orcid.org/0000-0002-2421-7859; Email: fsciktc@ku.ac.th

Yasuteru Shigeta − *Center for Computational Sciences, University of Tsukuba, Tsukuba, Ibaraki 305-8577, Japan;* orcid.org/0000-0002-3219-6007; Email: shigeta@ccs.tsukuba.ac.jp

Thanyada Rungrotmongkol − *Center of Excellence in Biocatalyst and Sustainable Biotechnology, Department of Biochemistry, Faculty of Science, Chulalongkorn University, Bangkok 10330, Thailand; Program in Bioinformatics and Computational Biology, Graduate School, Chulalongkorn University, Bangkok 10330, Thailand*; Email: Thanyada.r@chula.ac.th

Authors

Kowit Hengphasatporn − *Center for Computational Sciences, University of Tsukuba, Tsukuba, Ibaraki 305-8577, Japan;* orcid.org/0000-0001-8501-3844

Thitinan Aiebchun − *Center of Excellence in Biocatalyst and Sustainable Biotechnology, Department of Biochemistry, Faculty of Science, Chulalongkorn University, Bangkok 10330, Thailand*

Atima Auepattanapong − *Department of Chemistry and Center of Excellence for Innovation in Chemistry (PERCH-CIC), Faculty of Science, Mahidol University, Bangkok 10330, Thailand*

Onnicha Khaikate − *Department of Chemistry and Center of Excellence for Innovation in Chemistry (PERCH-CIC), Faculty of Science, Mahidol University, Bangkok 10330, Thailand*

Chutima Kuhakarn − *Department of Chemistry and Center of Excellence for Innovation in Chemistry (PERCH-CIC), Faculty of Science, Mahidol University, Bangkok 10330, Thailand;* orcid.org/0000-0003-4638-4356

Jatuporn Meesin − *Department of Chemistry, School of Science, King Mongkut's Institute of Technology Ladkrabang, Bangkok 10520, Thailand*

Complete contact information is available at: https://pubs.acs.org/10.1021/acsomega.3c01195

Author Contributions

○K.H. and T.A. contributed equally to this paper. K.H., Y.S., T.R., K.C., T.A., and P.M. conceived and designed the experiments. K.H. and T.A. conducted theoretical and experimental studies. A.A., O.K., J.M., and C.K. synthesized all of the compounds. T.A., P.M., T.R., K.C., and K.H. analyzed the data. K.H., T.A., and P.M. wrote the original manuscript. All authors reviewed and edited the manuscript to produce the final version.

Notes

The authors declare no competing financial interest.

ACKNOWLEDGMENTS

The authors acknowledge Supaphorn Seetaha and Lueacha Tabtimmai for guiding the bioassay. This research is funded by the Thailand Science Research and Innovation Fund, Chulalongkorn University (HEA662300073). P.M. thanks the Fundamental Fund of Khon Kaen University for financial support, and C.K. thanks the National Research Council of Thailand (NRCT) and Mahidol University: N42A650344 as well as the Center of Excellence for Innovation in Chemistry, Ministry of Higher Education, Science, Research and Innovation. K.H. and Y.S. were provided with computational resources through a high-performance computing infrastructure project (grant number hp200157) and Multidisciplinary Cooperative Research Program in CCS, University of Tsukuba. The QM calculations were funded by the Kakehashi project of the Tsukuba Innovation Arena (TIA) collaborative research program, CREST JST, Japan (grant number JP20338388), regarding the contribution by Y.S. Finally, K.C. received support for the bioassay from the Kasetsart University Research and Development Institute (KURDI)—grant number FF(KU)4.65.

REFERENCES

(1) Min, H.-Y.; Lee, H.-Y. Molecular targeted therapy for anticancer treatment. *Exp. Mol. Med.* **2022**, *54*, 1670−1694.

(2) Roskoski, R., Jr. The ErbB/HER family of protein-tyrosine kinases and cancer. *Pharmacol. Res.* **2014**, *79*, 34−74.

(3) Choowongkomon, K.; Carlin, C. R.; Sonnichsen, F. D. A structural model for the membrane-bound form of the juxtamembrane domain of the epidermal growth factor receptor. *J. Biol. Chem.* **2005**, *280*, 24043−24052.

(4) Flynn, J. F.; Wong, C.; Wu, J. M. Anti-EGFR therapy: Mechanism and advances in clinical efficacy in breast cancer. *J. Oncol.* **2009**, *2009*, No. 526963.

(5) Yang, C. H.; Chou, H. C.; Fu, Y. N.; Yeh, C. L.; Cheng, H. W.; Chang, I. C.; Liu, K. J.; Chang, G. C.; Tsai, T. F.; Tsai, S. F.; Liu, H. P.; Wu, Y. C.; Chen, Y. T.; Huang, S. F.; Chen, Y. R. EGFR overexpression in non-small cell lung cancers harboring EGFR mutations is associated with marked down-regulation of CD82. *Biochim. Biophys. Acta* **2015**, *1852*, 1540−1549.

(6) Hirsch, F. R.; Varella-Garcia, M.; Cappuzzo, F. Predictive value of EGFR and HER2 overexpression in advanced non-small-cell lung cancer. *Oncogene* **2009**, *28*, S32−S37.

(7) Hsu, P. C.; Jablons, D. M.; Yang, C. T.; You, L. Yes-Associated Protein (YAP) and the Regulation of Programmed Death-Ligand 1 (PD-L1) in Non-Small Cell Lung Cancer (NSCLC). *Int. J. Mol. Sci.* **2019**, *20*, No. 3821.

(8) Holbro, T.; Hynes, N. E. ErbB receptors: directing key signaling networks throughout life. *Annu. Rev. Pharmacol. Toxicol.* **2004**, *44*, 195−217.

(9) Wang, Y.; Schmid-Bindert, G.; Zhou, C. Erlotinib in the treatment of advanced non-small cell lung cancer: an update for clinicians. *Ther. Adv. Med. Oncol.* **2012**, *4*, 19−29.

(10) Bareschino, M. A.; Schettino, C.; Troiani, T.; Martinelli, E.; Morgillo, F.; Ciardiello, F. Erlotinib in cancer treatment. *Ann. Oncol.* **2007**, *18*, vi35−vi41.

(11) Yun, C.-H.; Mengwasser, K. E.; Toms, A. V.; Woo, M. S.; Greulich, H.; Wong, K.-K.; Meyerson, M.; Eck, M. J. The T790M mutation in EGFR kinase causes drug resistance by increasing the affinity for ATP. *Proc. Natl. Acad. Sci.* **2008**, *105*, 2070−2075.

(12) Becker, A.; van Wijk, A.; Smit, E. F.; Postmus, P. E. Side-effects of long-term administration of erlotinib in patients with non-small cell lung cancer. *J. Thorac. Oncol.* **2010**, *5*, 1477−1480.

(13) Tang, J.; Salama, R.; Gadgeel, S. M.; Sarkar, F. H.; Ahmad, A. Erlotinib resistance in lung cancer: current progress and future perspectives. *Front. Pharmacol.* **2013**, *4*, 15.

(14) Politi, K.; Fan, P. D.; Shen, R.; Zakowski, M.; Varmus, H. Erlotinib resistance in mouse models of epidermal growth factor receptor-induced lung adenocarcinoma. *Dis. Models Mech.* **2010**, *3*, 111−119.
(15) Chauhan, M.; Joshi, G.; Kler, H.; Kashyap, A.; Amrutkar, S. M.; Sharma, P.; Bhilare, K. D.; Chand Banerjee, U.; Singh, S.; Kumar, R. Dual inhibitors of epidermal growth factor receptor and topoisomerase IIα derived from a quinoline scaffold. *RSC Adv.* **2016**, *6*, 77717−77734.
(16) Martorana, A.; La Monica, G.; Lauria, A. Quinoline-based molecules targeting c-Met, EGF, and VEGF receptors and the proteins involved in related carcinogenic pathways. *Molecules* **2020**, *25*, No. 4279.
(17) George, R. F.; Samir, E. M.; Abdelhamed, M. N.; Abdel-Aziz, H. A.; Abbas, S. E. Synthesis and anti-proliferative activity of some new quinoline based 4,5-dihydropyrazoles and their thiazole hybrids as EGFR inhibitors. *Bioorg. Chem.* **2019**, *83*, 186−197.
(18) Meesin, J.; Pohmakotr, M.; Reutrakul, V.; Soorukram, D.; Leowanawat, P.; Saithong, S.; Kuhakarn, C. TBAI/TBHP-mediated cascade cyclization toward sulfonylated indeno[1,2-c]quinolines. *Org. Lett.* **2017**, *19*, 6546−6549.
(19) Xiong, G.; Wu, Z.; Yi, J.; Fu, L.; Yang, Z.; Hsieh, C.; Yin, M.; Zeng, X.; Wu, C.; Lu, A.; Chen, X.; Hou, T.; Cao, D. ADMETlab 2.0: an integrated online platform for accurate and comprehensive predictions of ADMET properties. *Nucleic Acids Res.* **2021**, *49*, W5−W14.
(20) Elkamhawy, A.; Farag, A. K.; Viswanath, A. N.; Bedair, T. M.; Leem, D. G.; Lee, K. T.; Pae, A. N.; Roh, E. J. Targeting EGFR/HER2 tyrosine kinases with a new potent series of 6-substituted 4-anilinoquinazoline hybrids: Design, synthesis, kinase assay, cell-based assay, and molecular docking. *Bioorg. Med. Chem. Lett.* **2015**, *25*, 5147−5154.
(21) Li, D. D.; Qin, Y. J.; Sun, J.; Li, J. R.; Fang, F.; Du, Q. R.; Qian, Y.; Gong, H. B.; Zhu, H. L. Optimization of substituted 6-salicyl-4-anilinoquinazoline derivatives as dual EGFR/HER2 tyrosine kinase inhibitors. *PLoS One* **2013**, *8*, No. e69427.
(22) Liu, W. J.; Liu, X. J.; Xu, J.; Li, L.; Li, Y.; Zhang, S. H.; Wang, J. L.; Miao, Q. F.; Zhen, Y. S. EGFR-targeting, beta-defensin-tailored fusion protein exhibits high therapeutic efficacy against EGFR-expressed human carcinoma via mitochondria-mediated apoptosis. *Acta Pharmacol. Sin.* **2018**, *39*, 1777−1786.
(23) Sangpheak, K.; Tabtimmai, L.; Seetaha, S.; Rungnim, C.; Chavasiri, W.; Wolschann, P.; Choowongkomon, K.; Rungrotmongkol, T. Biological evaluation and molecular dynamics simulation of chalcone derivatives as epidermal growth factor-tyrosine kinase inhibitors. *Molecules* **2019**, *24*, No. 1092.
(24) Janmaat, M. L.; Kruyt, F. A.; Rodriguez, J. A.; Giaccone, G. Response to epidermal growth factor receptor inhibitors in non-small cell lung cancer cells: limited antiproliferative effects and absence of apoptosis associated with persistent activity of extracellular signal-regulated kinase or Akt kinase pathways. *Clin. Cancer Res.* **2003**, *9*, 2316−2326.
(25) Demiray, A.; et al. The Frequency of EGFR and KRAS Mutations in the Turkish Population with Non-small Cell Lung Cancer and their Response to Erlotinib Therapy. *Balk. J. Med. Genet.* **2018**, *21*, 21−26.
(26) Park, J. H.; Liu, Y.; Lemmon, M. A.; Radhakrishnan, R. Erlotinib binds both inactive and active conformations of the EGFR tyrosine kinase domain. *Biochem. J.* **2012**, *448*, 417−423.
(27) Ferlenghi, F.; Scalvini, L.; Vacondio, F.; Castelli, R.; Bozza, N.; Marseglia, G.; Rivara, S.; Lodola, A.; La Monica, S.; Minari, R.; Petronini, P. G.; Alfieri, R.; Tiseo, M.; Mor, M. A sulfonyl fluoride derivative inhibits EGFRL858R/T790M/C797S by covalent modification of the catalytic lysine. *Eur. J. Med. Chem.* **2021**, *225*, No. 113786.
(28) Sangpheak, K.; Tabtimmai, L.; Seetaha, S.; Rungnim, C.; Chavasiri, W.; Wolschann, P.; Choowongkomon, K.; Rungrotmongkol, T. Biological evaluation and molecular dynamics simulation of chalcone derivatives as epidermal growth factor-tyrosine kinase inhibitors. *Molecules* **2019**, *24*, No. 1092.
(29) Mahalapbutr, P.; Leechaisit, R.; Thongnum, A.; Todsaporn, D.; Prachayasittikul, V.; Rungrotmongkol, T.; Prachayasittikul, S.; Ruchirawat, S.; Prachayasittikul, V.; Pingaew, R. Discovery of anilino-1,4-naphthoquinones as potent EGFR tyrosine kinase inhibitors: synthesis, biological evaluation, and comprehensive molecular modeling. *ACS Omega* **2022**, *7*, 17881−17893.
(30) Fischer, T.; Najjar, A.; Totzke, F.; Schächtele, C.; Sippl, W.; Ritter, C.; Hilgeroth, A. Discovery of novel dual inhibitors of receptor tyrosine kinases EGFR and PDGFR-β related to anticancer drug resistance. *J. Enzyme Inhib. Med. Chem.* **2018**, *33*, 1−8.
(31) Shen, J.; Zhang, T.; Cheng, Z.; Zhu, N.; Wang, H.; Lin, L.; Wang, Z.; Yi, H.; Hu, M. Lycorine inhibits glioblastoma multiforme growth through EGFR suppression. *J. Exp. Clin. Cancer Res.* **2018**, *37*, No. 157.
(32) Wang, E.; Sun, H.; Wang, J.; Wang, Z.; Liu, H.; Zhang, J. Z. H.; Hou, T. End-point binding free energy calculation with MM/PBSA and MM/GBSA: Strategies and applications in drug design. *Chem. Rev.* **2019**, *119*, 9478−9508.
(33) Sangpheak, K.; Tabtimmai, L.; Seetaha, S.; Rungnim, C.; Chavasiri, W.; Wolschann, P.; Choowongkomon, K.; Rungrotmongkol, T. Biological evaluation and molecular dynamics simulation of chalcone derivatives as epidermal growth factor-tyrosine kinase inhibitors. *Molecules* **2019**, *24*, 1092.
(34) Seetaha, S.; Ratanabanyong, S.; Choowongkomon, K. Expression, purification, and characterization of the native intracellular domain of human epidermal growth factor receptors 1 and 2 in Escherichia coli. *Appl. Microbiol. Biotechnol.* **2019**, *103*, 8427−8438.
(35) Stamos, J.; Sliwkowski, M. X.; Eigenbrot, C. Structure of the epidermal growth factor receptor kinase domain alone and in complex with a 4-anilinoquinazoline inhibitor. *J. Biol. Chem.* **2002**, *277*, 46265−46272.
(36) Frisch, M.; Trucks, G.; Schlegel, H. B.; Scuseria, G. E.; Robb, M. A.; Cheeseman, J. R.; Scalmani, G.; Barone, V.; Mennucci, B.; Petersson, G. J. I.; Wallingford, C. T. *Gaussian 09*, Revision d. 01; Gaussian 2009.
(37) Kammarabutr, J.; Mahalapbutr, P.; Nutho, B.; Kungwan, N.; Rungrotmongkol, T. Low susceptibility of asunaprevir towards R155K and D168A point mutations in HCV NS3/4A protease: A molecular dynamics simulation. *J. Mol. Graphics Modell.* **2019**, *89*, 122−130.
(38) Sanachai, K.; Mahalapbutr, P.; Choowongkomon, K.; Poo-Arporn, R. P.; Wolschann, P.; Rungrotmongkol, T. Insights into the binding recognition and susceptibility of tofacitinib toward janus kinases. *ACS Omega* **2020**, *5*, 369−377.
(39) Klaewkla, M.; Charoenwongpaiboon, T.; Mahalapbutr, P. Molecular basis of the new COVID-19 target neuropilin-1 in complex with SARS-CoV-2 S1 C-end rule peptide and small-molecule antagonists. *J. Mol. Liq.* **2021**, *335*, No. 116537.
(40) Wu, G.; Robertson, D. H.; Brooks, C. L., III; Vieth, M. Detailed analysis of grid-based molecular docking: A case study of CDOCKER-A CHARMm-based MD docking algorithm **2003** *24* 1549 1562 DOI: 10.1002/jcc.10306.
(41) Pettersen, E. F.; Goddard, T. D.; Huang, C. C.; Couch, G. S.; Greenblatt, D. M.; Meng, E. C.; Ferrin, T. E. UCSF chimera - A visualization system for exploratory research and analysis. *J. Comput. Chem.* **2004**, *25*, 1605−1612.
(42) Takaya, D.; Niwa, H.; Mikuni, J.; Nakamura, K.; Handa, N.; Tanaka, A.; Yokoyama, S.; Honma, T. Protein ligand interaction analysis against new CaMKK2 inhibitors by use of X-ray crystallography and the fragment molecular orbital (FMO) method. *J. Mol. Graphics Modell.* **2020**, *99*, No. 107599.
(43) Barca, G. M. J.; Bertoni, C.; Carrington, L.; Datta, D.; De Silva, N.; Deustua, J. E.; Fedorov, D. G.; Gour, J. R.; Gunina, A. O.; Guidez, E.; Harville, T.; Irle, S.; Ivanic, J.; Kowalski, K.; Leang, S. S.; Li, H.; Li, W.; Lutz, J. J.; Magoulas, I.; Mato, J.; Mironov, V.; Nakata, H.; Pham, B. Q.; Piecuch, P.; Poole, D.; Pruitt, S. R.; Rendell, A. P.; Roskop, L. B.; Ruedenberg, K.; Sattasathuchana, T.; Schmidt, M. W.; Shen, J.; Slipchenko, L.; Sosonkina, M.; Sundriyal, V.; Tiwari, A.; Galvez

https://doi.org/10.1021/acsomega.3c01195
ACS Omega 2023, 8, 19645−19655

Vallejo, J. L.; Westheimer, B.; Wloch, M.; Xu, P.; Zahariev, F.; Gordon, M. S. Recent developments in the general atomic and molecular electronic structure system. *J. Chem. Phys.* **2020**, *152*, No. 154102.
(44) Hengphasatporn, K.; Garon, A.; Wolschann, P.; Langer, T.; Yasuteru, S.; Huynh, T. N. T.; Chavasiri, W.; Saelee, T.; Boonyasuppayakorn, S.; Rungrotmongkol, T. Multiple virtual screening strategies for the discovery of novel compounds active against dengue virus: A hit identification study. *Sci. Pharm.* **2020**, *88*, 2.
(45) Boonyasuppayakorn, S.; Saelee, T.; Visitchanakun, P.; Leelahavanichkul, A.; Hengphasatporn, K.; Shigeta, Y.; Huynh, T. N.; Chu, J. J.; Rungrotmongkol, T.; Chavasiri, W. Dibromopinocembrin and dibromopinostrobin are potential anti-dengue leads with mild animal toxicity. *Molecules* **2020**, *25*, No. 4154.
(46) Hengphasatporn, K.; Wilasluck, P.; Deetanya, P.; Wangkanont, K.; Chavasiri, W.; Visitchanakun, P.; Leelahavanichkul, A.; Paunrat, W.; Boonyasuppayakorn, S.; Rungrotmongkol, T.; Hannongbua, S.; Shigeta, Y. Halogenated baicalein as a promising antiviral agent toward SARS-CoV-2 main protease. *J. Chem. Inf. Model.* **2022**, *62*, 1498−1509.
(47) Hengphasatporn, K.; Harada, R.; Wilasluck, P.; Deetanya, P.; Sukandar, E. R.; Chavasiri, W.; Suroengrit, A.; Boonyasuppayakorn, S.; Rungrotmongkol, T.; Wangkanont, K.; Shigeta, Y. Promising SARS-CoV-2 main protease inhibitor ligand-binding modes evaluated using LB-PaCS-MD/FMO. *Sci. Rep.* **2022**, *12*, No. 17984.

https://doi.org/10.1021/acsomega.3c01195
ACS Omega 2023, 8, 19645−19655